Research Article

K. A. Mahmoud, Mazen M. Binmujlli, M. W. Marashdeh*, Mamduh J. Aljaafreh, Ahmad Saleh, and M. Y. Hanfi*

Gamma-ray shielding analysis using the experimental measurements for copper(II) sulfate-doped polyepoxide resins

https://doi.org/10.1515/epoly-2023-0142
received September 14, 2023; accepted November 16, 2023

Abstract: The present work aims to study the effect of the $CuSO_4$ additive on the physical and radiation-shielding properties of polyepoxide resins. As a result, a series of four samples with the chemical composition $x CuSO_4$ + (100 − x) (epoxy resin and hardener) was synthesized. The fabrication of samples was performed under atmospheric pressure and at room temperature. The density of the fabricated $CuSO_4$-doped polyepoxides resin was measured experimentally using an MH-300A densimeter with an accuracy of 0.001 mg·cm^{-3}. A narrow beam transmission method with an NaI (Tl) detector was used to evaluate and describe the effect of $CuSO_4$ on the linear attenuation coefficient of the fabricated composites in the γ-ray energy interval, which ranged between 33 and 1,332 keV. The estimated results showed a high enhancement in the μ values that increased from 0.259 to 1.749 cm^{-1}, raising the $CuSO_4$ concentration from 0 to 40 wt% at a γ-photon energy of 33 keV. The enhancement in the μ values decreased with an increase in the γ-photon energy to 1,332 keV, whereas the μ values increased from 0.077 to 0.102 cm^{-1} with an increase in the $CuSO_4$ concentration between 0 and 40 wt%, respectively. This showed that increased μ values positively affected the half-value thickness ($\Delta_{0.5}$, cm), mean free path (λ, cm), lead equivalent thickness (Δ_{eq}, cm), and the transmission factor (%); all of the mentioned parameters suffer a considerable decrease with increasing $CuSO_4$ concentration between 0 and 40 wt%.

Keywords: shielding properties, polyepoxides resin, copper(II) sulfate, narrow beam transmission method

1 Introduction

Radiation is a type of energy that originates from a source, travels across space, and has the potential to penetrate a variety of materials. Ionizing radiation and nonionizing radiation are the two basic classifications of radiation based on their capacity to ionize materials (1,2). Nonionizing radiation like visible light, radio waves, and microwaves do not have enough energy to pick up electrons from the atom (3). Ionizing radiation is electromagnetic radiation that has a higher energy than nonionizing radiation, enabling it to eject electrons from atoms and generate ions. Ionizing radiation is made up of various particles and photons, like X-rays, γ rays, alpha, beta, etc. (4). The use of high-energy ionizing radiation, particularly γ-radiation, is growing swiftly in a variety of disciplines, covering industries, nuclear reactors, medical diagnostics, nuclear research facilities, food irradiation, nuclear waste storage sites, biological investigations, defect detection in casting processes, nuclear medical imaging and therapy, space exploration, high-energy physics experiments, etc. (5,6).

Because γ-rays are so powerful and piercing, unintentional exposure to them can have negative effects on humans, the environment, and other objects. Additionally, this may

*** Corresponding author: M. W. Marashdeh**, Department of Physics, College of Sciences, Imam Mohammad Ibn Saud Islamic University (IMSIU), Riyadh, 11623, Saudi Arabia, e-mail: mwmarashdeh@imamu.edu.sa
*** Corresponding author: M. Y. Hanfi**, Department of Medical and Radiation Research, Research Sector, Nuclear Materials Authority, 530 Maadi, Cairo, Egypt; Department of Life Safety, Institute of Fundamental Education, Ural Federal University, Ekaterinburg 620002, Russia, e-mail: mokhamed.khanfi@urfu.ru, m.nuc2012@gmail.com
K. A. Mahmoud: Department of Chemical Analysis, Production Sector, Nuclear Materials Authority, 530 Maadi, Cairo, Egypt; Department of Nuclear Power Plants and Renewable Energy Sources, Ural Power engineering institute, Ural Federal University, Ekaterinburg 620002, Russia
Mazen M. Binmujlli: Department of Internal Medicine, College of Medicine, Imam Mohammad Ibn Saud Islamic University (IMSIU), Riyadh, 11623, Saudi Arabia
Mamduh J. Aljaafreh: Department of Physics, College of Sciences, Imam Mohammad Ibn Saud Islamic University (IMSIU), Riyadh, 11623, Saudi Arabia
Ahmad Saleh: Department of Mathematics and Natural Sciences, Prince Mohammad Bin Fahd University, Al Khobar, 31952, Saudi Arabia

result in radiation sickness, organ damage, cancer, cell mutations, component failure, and other undesirable effects in humans (7). Thus, a specific focus is required for the creation of innovative γ-ray protective materials. Along with the employees' proximity to the radioactive isotopes, one must also take into account the energy and activity concentration of the radioactive sources (8). The two well-known radiation shields with the highest densities are concrete and steel (9); however, they are unbending and inflexible. As a result, these materials are ideal for shielding applications involving radioactive sources, nuclear power plants (NPPs), and rooms. Recently, several studies detailed the usage of various materials for radiation shielding in NPPs, hospitals, and X-ray facilities, including concrete, glasses, ceramics, and alloys (10–12).

Polymers typically have fairly poor mechanical properties but their flexibility makes them helpful in applications where this property is needed. They typically deform under heavy loads and strain. By introducing inorganic particles via reinforcing processes, mechanical qualities like tensile strength, modulus, or stiffness can be improved (13).

By adjusting the volume percentage, shape, and size of the filler particles, these qualities can be customized. The reinforcement of nanofillers with a very large aspect ratio and stiffness in a polymer matrix can result in superior improvement in mechanical characteristics (14).

Many researchers have recently worked to create innovative solutions for trash recycling and treatment involving polymer composite materials (15). To create ecologically friendly and sustainable materials, recycling and the addition of various filler elements to recycled polymers that can be composted easily (16) are crucial (17). There have been numerous attempts to use biodegradable fillers that can also improve the performance of the composite (18,19). Other researchers were focused on creating thermoplastic composites using recyclable fibers to reduce the usage of fillers while preserving a healthy, clean environment (20,21).

The current work is novel in that it aims to create a new non-expensive lightweight polymer composite that can attenuate low- and intermediate-energy γ-ray photons and test its ability to withstand γ-ray energies emitted by radioactive isotopes used in medical and industrial applications.

2 Materials and methods

2.1 Sample preparation

The copper ions showed better radiation-shielding properties than Fe ions and other heavy metallic ions. Therefore, the ability of $CuSO_4$ powder to enhance the γ-ray shielding properties of epoxy materials was investigated. A series of polyepoxide resins consisting of four samples was reinforced with various concentrations of the $CuSO_4$ compound (the purity of $CuSO_4$ was ≈99.95%, and was supplied by Himreactiv, Yekaterinburg, Russia). The equation (100 − x) (part A + part B) + xPbO, where x = 0%, 10%, or 40% by weight, demonstrated the chemical composition of the four samples, where part A is the polyepoxides resin, while part B is the curing agent. Additionally, SlabDOC (Ivanovo, Russia) with a purity of 98% supplies the epoxy (parts A and B). The required amounts from each component constituting the composite (part A, part B, and $CuSO_4$) were determined accurately using an electronic balance with an accuracy of ±0.01 mg. For all fabricated composites, the resin-to-curing agent was kept constant at 2:1. A vertical blender was used to mix the composite components for 15 min. After that, the mixture was cast in a silicon cylindrical mold with dimensions of 3 cm × 3 cm. The solidification of the synthesized samples was performed at room temperature overnight. The density of the fabricated concrete was determined using a MXBAOHENG MH-300A density meter (Guangdong, China) and the immersing liquid was water with a density $\rho_L \approx 1\,g{\cdot}cm^{-3}$, according to the Archimedes principle (see Eq. 1). The uncertainty in the density measurements was $\pm 0.001\,g{\cdot}cm^{-3}$ (22,23).

$$\text{Density}\left(\rho_{\text{composite}}, g{\cdot}cm^{-3}\right) = \frac{(W_a - W_L)}{W_a}\rho_L \tag{1}$$

where W_a and W_L are the weight of the composite in the dry air and immersing liquid, respectively.

2.2 Structural characterization

The characterization of the polymer samples was performed using X-ray diffraction (XRD)(Malvern Panalytical Empyrean device model, 2020, Netherlands). About 200 mg of each sample was pounded by hand (an agate mortar) to reach a powder size of 0.1 mm. Then, a continuous scan was applied with 0.03 step size (2θ) at 40 kV and 30 mA for a tube of Cu target and Ni filter.

A scanning electron microscope (SEM; Thermo Scientific Prisma E, USA), assisted with the EDX device, was used to determine the chemical composition (Table 1) of the studied polyepoxide-doped $CuSO_4$ composites as well as its morphological characteristics. SEM images were captured using an accelerating voltage of 30 kV and a magnification factor of 300×.

2.3 γ-ray shielding evaluation

The γ-ray shielding properties were evaluated experimentally using the narrow beam transmission method and a

Table 1: Chemical composition of the fabricated composites as detected by EDX spectroscopy

	E-Cu0%	Chemical composition (wt%)		
		E-Cu10%	E-Cu20%	E-Cu40%
C	63.7	59.3	56.6	42.8
O	36.1	35.4	37	46.8
S	0	0.1	2	2.8
Cl	0.2	0.2	0.1	0.1
Cu		2.1	4.3	7.6
ρ (g·cm^{-3})	1.127 ± 0.022	1.186 ± 0.023	1.271 ± 0.025	1.424 ± 0.028

NaI (Tl) detector, as illustrated in Figure 1. The count for radioactive sources (Ba-133, Na-22, Cs-137, and Co-60) was detected before and after using the fabricated composites. Moreover, the thickness of the fabricated composites was measured using a micrometer with an uncertainty of 0.01 µm. The linear attenuation coefficient (μ, cm^{-1}) represents the slope of the relation between the experimentally measured counts Ln(N_o/N_t) and the composite thickness (24,25):

$$\mu \quad (\mathrm{cm}^{-1}) = \frac{\mathrm{I}}{x} \ln\left(\frac{N_o}{N_t}\right) \tag{2}$$

where N_o and N_t are the total emitted photon number and transmitted photon number, respectively. The mass attenuation coefficient (μ_m, cm^2·g^{-1}) can be determined according to Eq. 3 based on the μ and ρ material values:

$$\mu_m \quad (\mathrm{cm}^2\cdot\mathrm{g}^{-1}) = \frac{\mu(\mathrm{cm}^{-1})}{\rho_{composite}(\mathrm{g}\cdot\mathrm{cm}^{-3})} \tag{3}$$

The thickness required to absorb half of the applied γ-photons is known as the half-value thickness ($\Delta_{0.5}$, cm), where it is inversely proportional to the μ value, as illustrated in Eq. 4. Additionally, the transmission factor (TF, %) and the radiation protection efficiency (RPE, %) for the fabricated composites can be determined based on the recorded values of N_o, N_t, and N_a, according to Eqs. 5 and 6:

$$\Delta_{0.5} \quad (\mathrm{cm}) = \frac{\ln(2)}{\mu} \tag{4}$$

$$\mathrm{TF}(\%) = \frac{N_t}{N_o} \times 100 \tag{5}$$

$$\mathrm{RPE}(\%) = \frac{N_a}{N_o} \times 100 \tag{6}$$

3 Results and discussion

3.1 Physical properties

The density of the fabricated composites was measured experimentally, as illustrated in Figure 2. The $CuSO_4$ compound partially replaced the epoxy (polyepoxides resin and hardener) in the composites, which made the composites denser. The density increased by a factor of 26.35%,

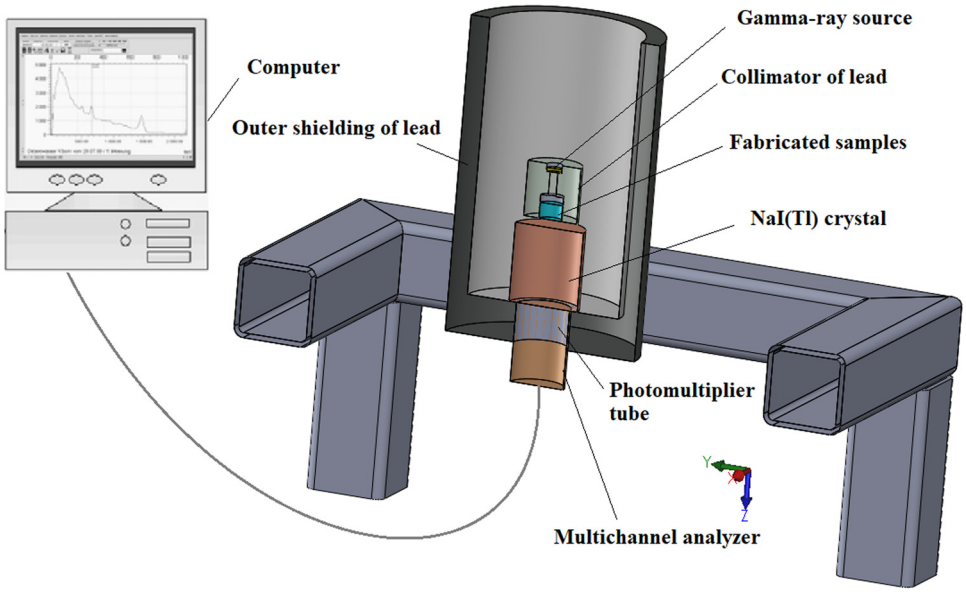

Figure 1: The experimental setup for the experimental measurements.

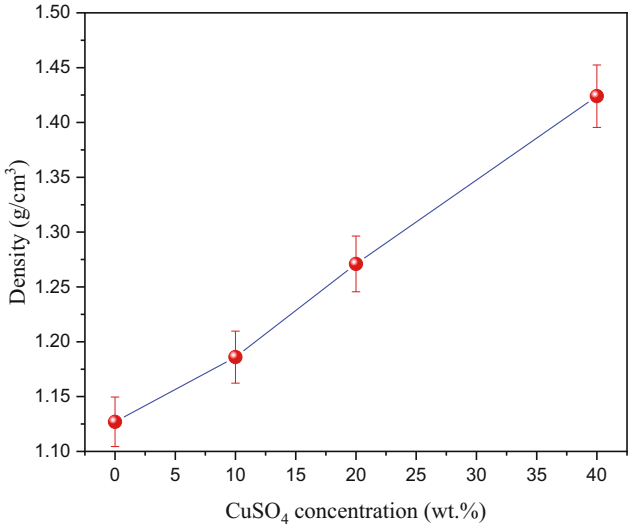

Figure 2: The variation of the fabricated polymetric samples *versus* $CuSO_4$ concentrations.

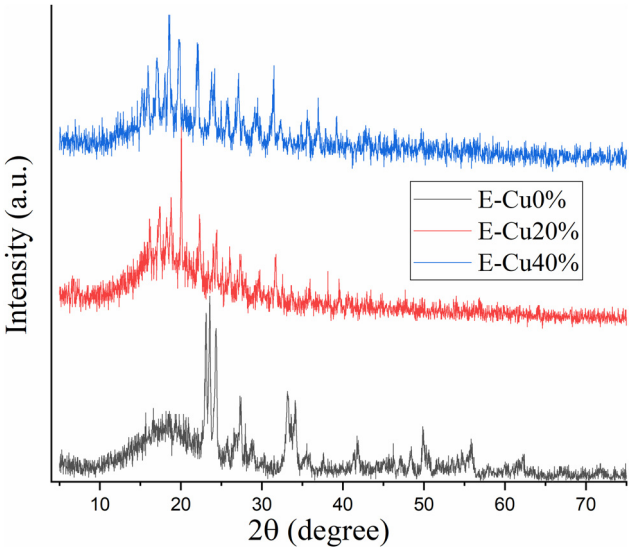

Figure 3: XRD diffraction pattern of epoxy (E-Cu0%) and epoxy-reinforced $CuSO_4$ composites (E-Cu10% and E-Cu20%).

where it increased from 1.127 to 1.424 g·cm^{-3} with an increase in the $CuSO_4$ concentration from 0 to 40 wt%. This increase is due to the partial replacement of the light epoxy material with a density of 1.127 g·cm^{-3} by dense $CuSO_4$ (ρ = 3.65 g·cm^{-3}).

3.2 XRD

XRD is a powerful technique that can be used to characterize the structure and properties of materials. It is a valuable tool for studying the interaction between polymers and other materials (26). The XRD pattern of a polymer doped with 10% and 40% $CuSO_4$ is similar, but the intensity of 40% $CuSO_4$ peaks is high compared to the sample with 10% $CuSO_4$ (Figure 3). This behavior is attributed to the concentration of $CuSO_4$ in the sample. The position of the $CuSO_4$ peaks is the same for both samples, and no shift in 2θ values is detected; moreover, the crystal structure of $CuSO_4$ is the same regardless of the concentration. The presence of $CuSO_4$ peaks in the XRD pattern indicates that $CuSO_4$ has been successfully doped into the polymer. The intensity of the $CuSO_4$ peaks can be used to determine the concentration of $CuSO_4$ in the sample. Here is an example of the XRD pattern of a polymer doped with 10% $CuSO_4$ concentration: the X-ray diffraction pattern matches with PDF-Card No (72-1299) of copper sulfate hydrate ($CuSO_4$ $(H_2O)_5$). The most intense peak appears at 2θ = 19.95° with a *d*-spacing of 4.44 Å. However, the PDF-Card No (76-689) of copper sulfate hydrate ($CuSO_4(H_2O)_3$): the most intense peak appears at 2θ = 18.63° with a *d*-spacing of 4.75 Å (27). The XRD pattern of a polymer-doped $CuSO_4$ can be used to study the crystal structure of t $CuSO_4$, the concentration of $CuSO_4$ in the sample, and the interaction between the $CuSO_4$ and the polymer. The presence of new peaks in the XRD pattern may indicate that $CuSO_4$ has caused the polymer to crystallize or that it has created new defects in the polymer (28).

The chemical composition obtained from SEM-EDX for the fabricated polyepoxides-reinforced $CuSO_4$ composites shows an increase in the Cu concentrations by increasing the $CuSO_4$ doping ratio in the fabricated composites. The increase in the Cu concentration is accompanied by a reduction in the C and O concentrations, which consisted of the pure polyepoxide resin (Table 1). Therefore, the EDX spectra affirm the diffusion of $CuSO_4$ fillers in the fabricated samples, as well as the presence of polyepoxide resin, and traces of Ca, Ti, and Ni in the samples.

The backscattered electron images of the investigated samples show the distribution of the $CuSO_4$ composites within the fabricated composites, as illustrated in Figure 4. The SEM images showed an increase in the filler particles with an increase in the $CuSO_4$ concentration; moreover, the grain size of the filler particles varied up to 22 µm.

3.3 Radiation shielding capacity

The linear attenuation coefficient measures and predicts the capacity of the current polymer to attenuate the incoming photon energy. The intensity of incoming photons affected the variation in polymer composite thickness. Figure 5

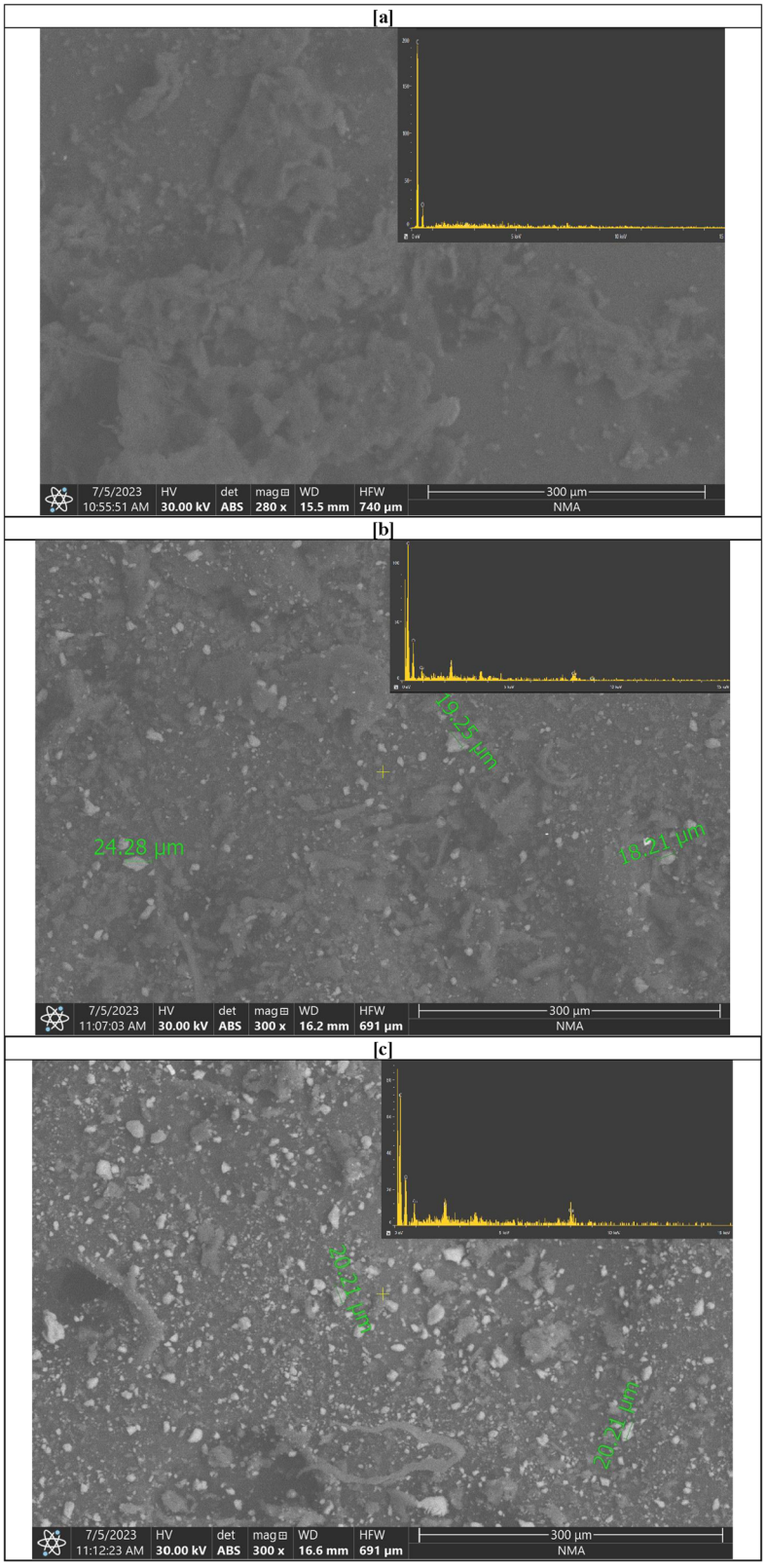

Figure 4: SEM and EDX analysis for the fabricated epoxy-based $CuSO_4$ composites. (a) E-Cu0%, (b) E-Cu20%, and (c) E-Cu40%.

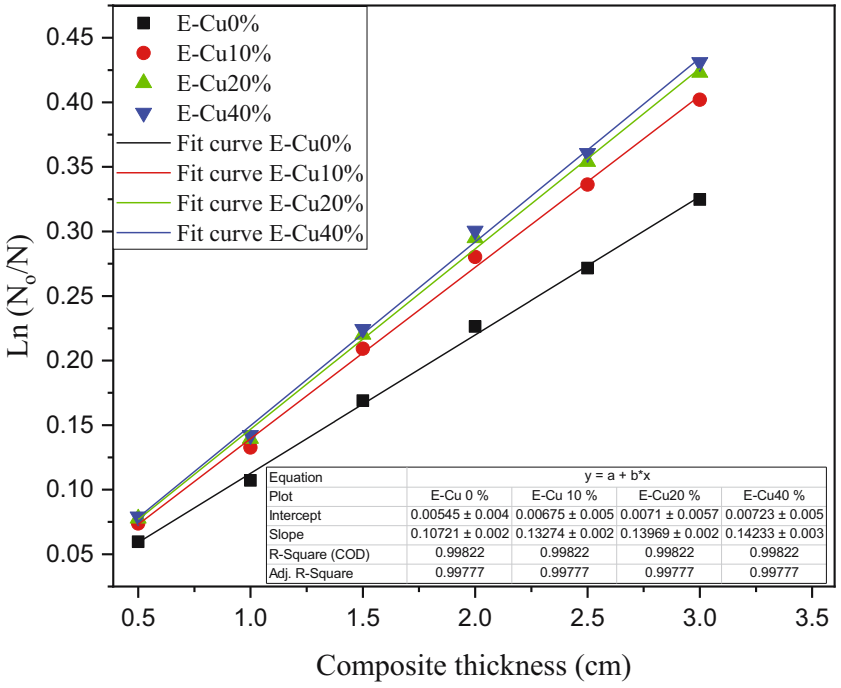

Figure 5: Variation of the ln(N_o/N) *versus* the composite thickness (cm).

illustrates that the transmitted intensity of the incoming photon affects the thickness of the polymer composites, which increased from 0.5 to 5 cm. This variation is due to the ability of the polymer composites (E-Cu) to decrease the intensity of the incoming photons and allow part of them to pass and transmit through the composite materials (slope). This is called the linear attenuation coefficient. We can observe in Figure 5 that the linear attenuation coefficient values varied from 0.10 to 0.14 cm for E-Cu0% and E-Cu40%, respectively.

Figure 6 shows the changes in the linear attenuation coefficients of the investigated polymer composites depending on the energy of the photons that hit them. The linear attenuation coefficient values of the E-Cu composites decrease when the incoming photon energy increases from 33 to 1,332 keV. At a minimum energy range of 33–662 keV, the incoming γ-photons interact with the polymer composites and attenuate a large amount of the photons, while the rest penetrate the materials. In this range of energy, the dominant interaction is a photoelectric effect (PE), and its cross-section is inversely proportional to the incoming photon energy I. With the increase in the incoming photon energy, the μ values are diminished due to the second type of interaction called Compton scattering (CS). Through the CS interaction, some of the incoming γ photons are slowed down inside the polymer composites, while the rest have enough energy to go outside the material, where the cross-section (CS $\propto ZE^{-1}$) is measured. At high γ photon energies, the interaction will be governed by the pair production (PP) phenomenon, where the result of the interaction is two electrons. Figure 6 reveals that at a low photon energy of 33 keV, the maximum values of μ vary from 0.259 to 1.749 cm^{-1} for the polymer composites E-Cu0% and E-Cu40%, respectively. At a high photon energy of 1,332 keV, minimum μ values between 0.077 and 0.10 cm^{-1} are obtained for the polymer composites E-Cu0% and E-Cu40%, respectively.

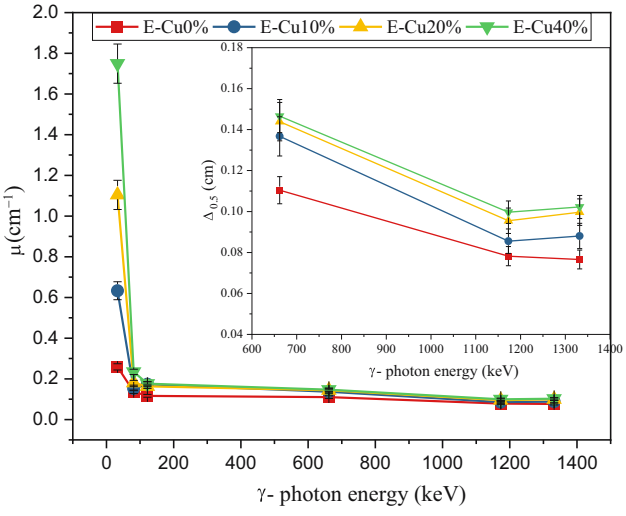

Figure 6: Dependence of the linear attenuation coefficient (μ, cm^{-1}) on the incident γ-photon energy.

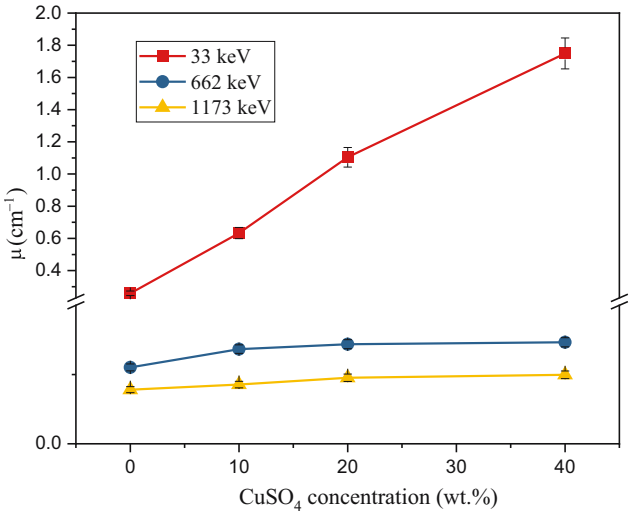

Figure 7: Variation of μ values *versus* $CuSO_4$-doping concentrations.

The second effect of the μ values is the variation of $CuSO_4$ in the polymer composites (Figure 7). The addition of $CuSO_4$ to the polymer composites leads to an improvement in their physical properties. The compactness of the polymer composite molecules increased, and the interactions between the incoming photons and the molecules of materials increased. Thus, the polymer composites have the ability to attenuate the incoming γ photons. Figure 7 shows the results of tests that changed with the concentration of $CuSO_4$ at three different incoming γ energies: 33, 662, and 1,173 keV. The lowest experimental values of the μ are 0.259, 0.107, and 0.078 cm^{-1} at 33, 662, and 1,173 keV, respectively, with a low $CuSO_4$ concentration of 0 wt%, while the highest values are 0.259, 0.107, and 0.078 cm^{-1} at 33, 662, and 1,173 keV, respectively, with a high $CuSO_4$ concentration of 40 wt%.

The mass attenuation coefficient (μ_m, $cm^2 \cdot g^{-1}$) for the fabricated E-Cu composites was evaluated based on the experimental μ values as well as the measured density for the synthesized composites. The μ_m values increased with increasing concentration of the additive $CuSO_4$, yielding0.0980, 0.1153, 0.1132, and 0.1030 $cm^2 \cdot g^{-1}$, respectively, for E-Cu0%, E-Cu10%, E-Cu20%, E-Cu40% composites, at a γ-ray energy of 662 keV. In order to validate the shielding capacity of the fabricated E-Cu composites, the aforementioned μ_m values were compared to those of some polymetric composites (29–38), as demonstrated in Figure 8. According to the comparative results shown in

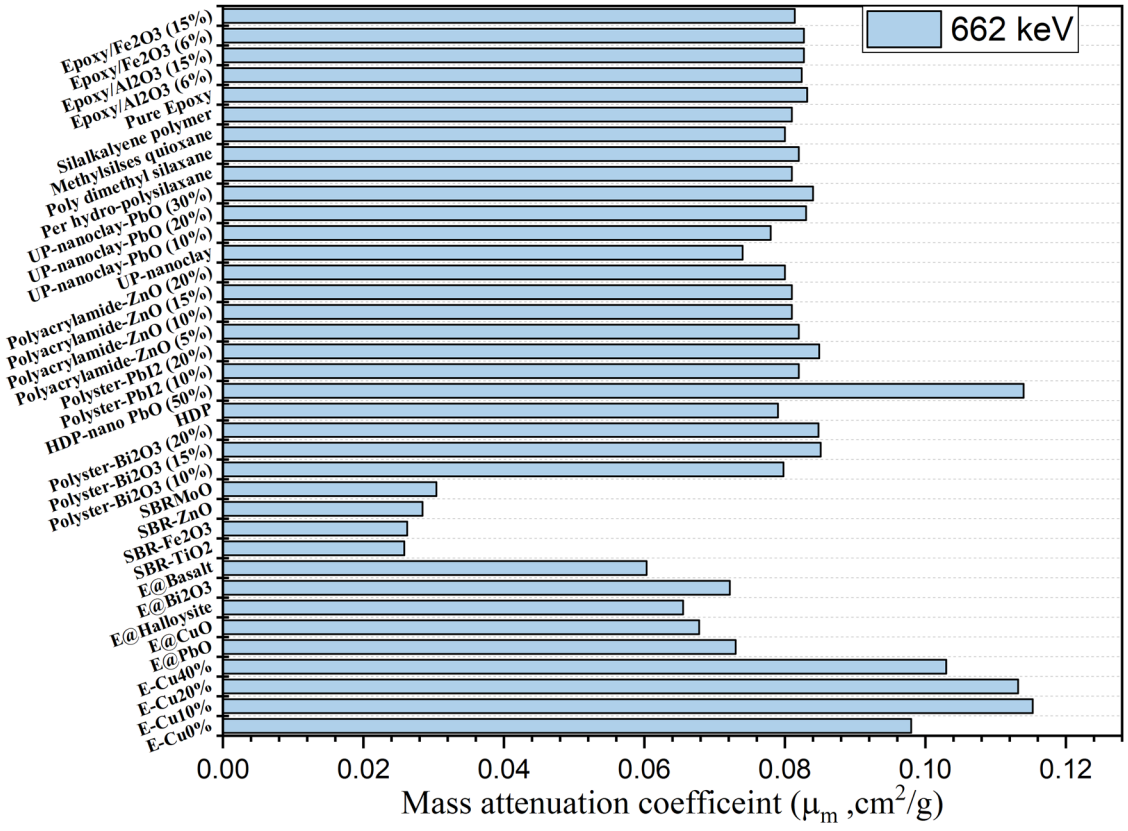

Figure 8: Comparison between the mass attenuation coefficient (μ_m, $cm^2 \cdot g^{-1}$) of the fabricated E-Cu composites and those of previously reported polymetric composites.

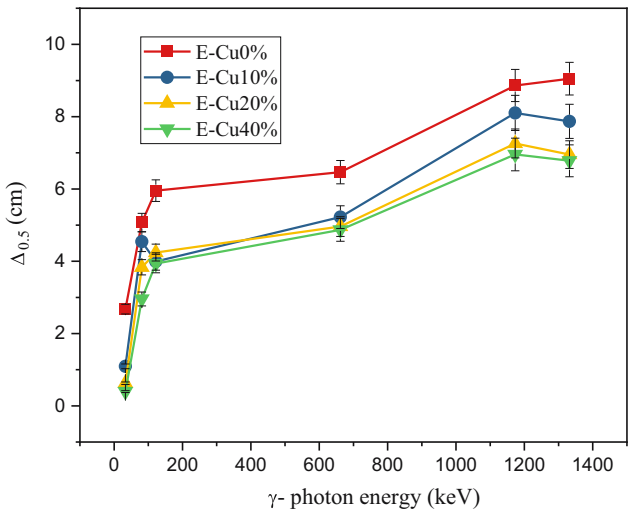

Figure 9: Variation of the half-value thickness ($\Delta_{0.5}$, cm) values *versus* the incident γ-photon energy.

Figure 8, the highest μ_m values were recorded for HDP nano-PbO (50%), with an m value of 0.1140 $cm^2 \cdot g^{-1}$, at a γ-photon energy of 662 keV. The fabricated composites in the current study have μ_m values better than that reported for composites E@PbO, E@CuO, E@Halloysite, E@Bi_2O_3, E@Basalt, SBR-TiO_2, SBR-Fe_2O_3, SBR-ZnO, SBRMoO, polyster-Bi_2O_3 (10%), polyster-Bi_2O_3 (15%), polyster-Bi_2O_3 (20%), HDP, polyster-PbI2 (10%), polyster-PbI2 (20%), polyacrylamide-ZnO (5%), polyacrylamide-ZnO (10%), polyacrylamide-ZnO (15%), polyacrylamide-ZnO (20%), UP-nanoclay, UP-nanoclay-PbO (10%), UP-nanoclay-PbO (20%), UP-nanoclay-PbO (30%), Per hydro-polysilaxane, Polydimethyl silaxane, methylsilses quioxane, silalkalyene polymer, pure epoxy, epoxy/Al_2O_3 (6%), epoxy/Al_2O_3 (15%), epoxy/Fe_2O_3 (6%), epoxy/Fe_2O_3 (15%) with μ_m values of 0.0730, 0.0678, 0.0655, 0.0722, 0.0603, 0.0258, 0.0262, 0.0284, 0.0304, 0.0798, 0.0851, 0.0848, 0.0790, 0.0820, 0.0849, 0.0820, 0.0810, 0.0810, 0.0800, 0.0740, 0.0780, 0.0830, 0.0840, 0.0810, 0.0820, 0.0800, 0.0810, 0.0832, 0.0824, 0.0827, 0.0827, and 0.0814 $cm^2 \cdot g^{-1}$, respectively, at 662 keV.

Compared to Figure 6, Figure 9 shows that the half-value layer ($\Delta_{0.5}$) values increase with the increase in the incoming γ-photon energy from 33 to 1,332 keV. The polymer composite material has enough resistance to reduce the incoming photon energy to half through the interactions. At constant $CuSO_4$ concentrations, the $\Delta_{0.5}$ values changed gradually with increasing incoming γ-photon energy. The variation of the highest $\Delta_{0.5}$ values is between 2.68 and 9.05 cm at zero $CuSO_4$ concentrations (E-Cu0%). This clarifies that the polymer composites with zero $CuSO_4$ concentrations do not have enough resistance to diminish the incoming γ-photon energy to a half through interactions with PE, CS, and PP. In contrast, when the concentration of $CuSO_4$ inside the polymer composites increases from 10% to 40%, the 0.5 values decrease. At a high $CuSO_4$ concentration (E-Cu40%), the minimum values range from 0.40 to 6.78 cm.

Figure 10 shows the mean free path (λ, cm) and the lead equivalent thickness (Δ_{eq}, cm) measured experimentally (for example, when the incoming energy of a γ photon is 81 keV). Figure 10 demonstrates the variation of λ and Δ_{eq}

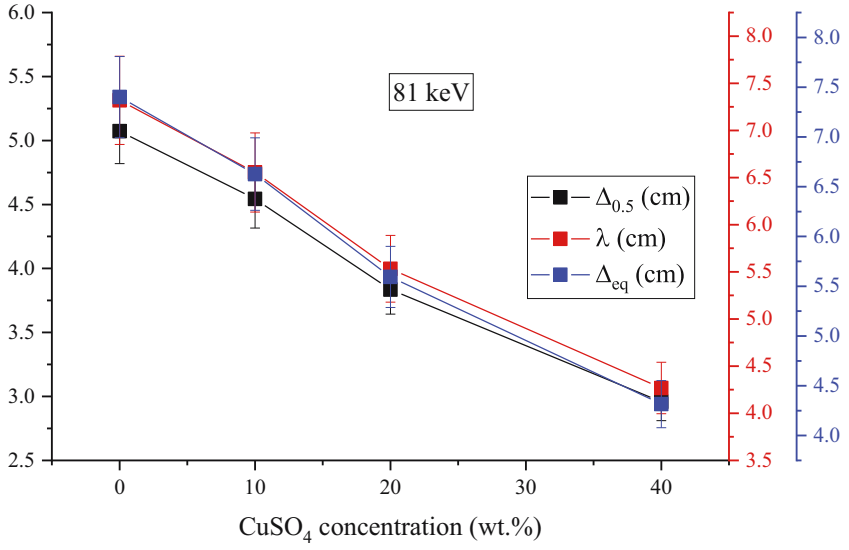

Figure 10: Dependence of the half-value thickness ($\Delta_{0.5}$, cm), mean free path (λ, cm), and lead equivalent thickness (Δ_{eq}, cm) *versus* $CuSO_4$ concentrations.

values with e $CuSO_4$ concentrations, where the λ values decrease from 7.32 to 4.27 cm. This decrease is because the number of collisions is lower when the concentration of $CuSO_4$ in the polymer composites increases from 10% to 40%. As a result, the γ photons' capacity to permeate the polymer composite materials also increases.

The Δ_{eq} values are calculated to describe the equivalent thickness of the polymer composite material that can be applied to obtain the same performance of lead to attenuate the incoming γ photons. The variations between the Δ_{eq} values and the incoming photon energies are graphically presented in Figure 10. As illustrated in Figure 10, the Δ_{eq} values decrease with an increase in the $CuSO_4$ concentrations from 10% to 40% inside the synthetic polymer composites. This decrease is observed in the PE interaction, where the decrease in μ values of pure Pb is higher than the calculated μ values of the fabricated polymer composites. For instance, the Δ_{eq} values reduced from 7.40 to 4.32 cm when $CuSO_4$ doping increased from 0% to 40%.

The TF of the synthetic polymer composites was computed and is presented in Figure 7. Figure 7 shows the changes in TF as the energy of the incoming γ photons increases from 33 to 1,332 keV at different concentrations of $CuSO_4$. The TF values decrease from 66% to 7% at a low γ energy of 33 keV with an increase in the concentration of $CuSO_4$ from 0% to 40%. Under the application of a low γ energy range, the γ photons interact inside the polymer composites, and the dominant interaction is PE. Therefore, the γ photons do not have the energy to transmit through the polymer composite material. Consequently, the TF will decrease with an increase in the percentage of $CuSO_4$ concentrations. As the energy of the incoming γ photons increases, CS interactions become more common. Hence, a small amount of γ energy can be used to collect photons inside the polymer composite material. Figure 11 also shows the RPE values with the increasing incoming γ-photon energy of the polymer composites. The incoming photons with high energies will penetrate the polymer composite materials, and the RPE values will be diminished. For example, at a low γ energy of 33 keV, the RPE alternated between an increase of 33% and 92% for the E-Cu0% and E-Cu40%, respectively, while with the application of high γ energy (1,332 keV), the RPE values decreased and changed between 11% and 14% for the E-Cu0% and E-Cu40%, respectively.

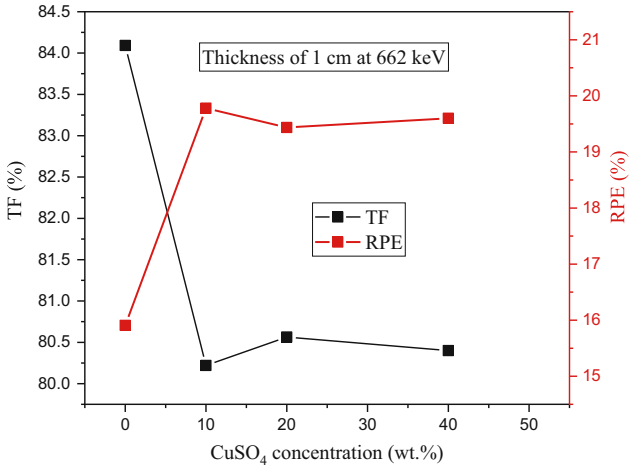

Figure 12: Variation of the transmission values (TF%) and radiation protection efficiency (RPE%) *versus* the $CuSO_4$ concentration at a γ-photon energy of 662 keV.

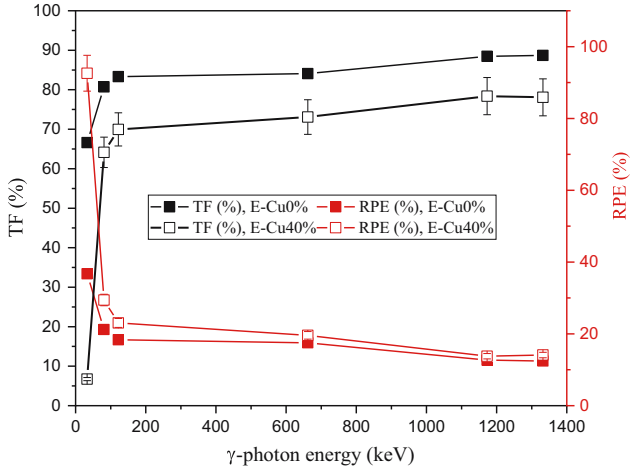

Figure 11: Variation of the transmission values (TF%) and radiation protection efficiency (RPE%) *versus* the incident γ-photon energy for E-Cu0% and E-Cu40% samples.

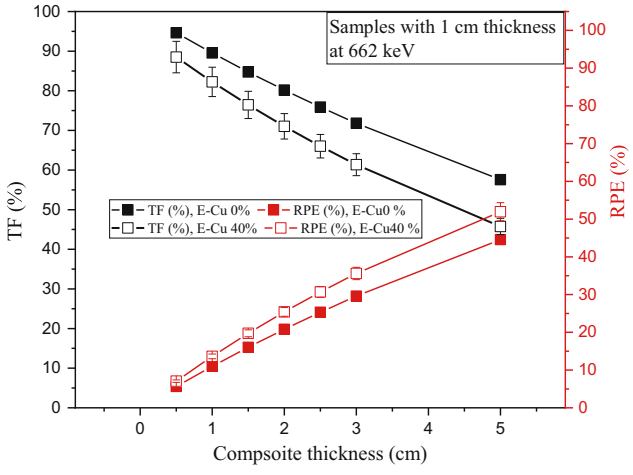

Figure 13: Dependence of the transmission values (TF%) and radiation protection efficiency (RPE%) on the fabricated composites thickness (cm) at a γ-photon energy of 662 keV.

Figure 12 shows the changes in TF and RPE values when $CuSO_4$ is added to the polymer composites studied with a thickness of 1 cm and a γ-photon energy of 662 keV. TF and RPE values have inverse relations with the increasing concentrations of $CuSO_4$ in the polymer composites. When the $CuSO_4$ concentrations increased from 0% to 40%, the TF values decreased from 84% to 80% and RPE increased from 16% to 20%. This increase in the RPE values, which leads to the polymer composite material, will impulse the γ photons to escape outside (i.e., N_a increase). Therefore, the transmission rate will decrease (i.e., N_t decrease) with the increase of $CuSO_4$ concentrations.

Figure 13 manifests the mutation of TF and RPE data by elevating the thickness of the polymer composite materials from 0.5 to 5 cm. Two polymer composites with $CuSO_4$ concentrations of 0% and 40% with a constant γ energy (662 keV) were used to study this change. The thickness of the polymer composites has a significant effect on the TF and RPE values. γ photons can easily pass through composite materials with a thickness of 0.5 cm and a low impulse. For E-Cu0% and E-Cu40%, the TF values drop from 95% to 92% and the RPE increases from 5% to 7%. With the increased thickness of the composites, the γ photons will make a lot of interactions, and their transmission (TF) decreases, accompanied by an increase in the impulse (RPE) of the polymer composite material.

4 Conclusion

Because of the high γ-ray interaction cross-section for Cu, it is utilized in the current study to modify the radiation shielding properties of polyepoxide resins. Therefore, a series of four polyepoxide resins reinforced with various concentrations of $CuSO_4$ was created. According to the density experimental examination, the addition of $CuSO_4$ contents to the polyepoxide resin enhances its density where the synthesized composites' density increased by 26% when the $CuSO_4$ concentration changed from 0 to 40 wt% in the synthesized composites. Additionally, the experimental examination of the fabricated composites shielding capacity shows an enhancement in their linear attenuation coefficient with an increase in the $CuSO_4$ concentration within the fabricated composites. The fabricated composites' linear attenuation coefficient enhanced by 71.48%, 51.27%, 32.76%, 27.43%, and 33.50% at γ-photon energies of 81, 122, 662, 1,173, and 1,332 keV, respectively, when the $CuSO_4$ concentration increased from 0 and 40 wt%. The enhancement in the linear attenuation coefficient decreased the $\Delta_{0.5}$, λ, Δ_{eq}, and TF values. The current synthesized composites have good shielding capacity and can be used in shielding low and intermediate γ-ray energies in γ knife, radiotherapy, and X-ray rooms, according to the comparison of the mass attenuation coefficient of the fabricated composites with the previously reported polymetric material.

Acknowledgement: This work was supported and funded by the Deanship of Scientific Research at Imam Mohammad Ibn Saud Islamic University (IMSIU) (grant number IMSIU RG23105).

Author contributions: All authors contributed equally to the manuscript.

Conflict of interest: The authors declare that they have no conflict of interest.

Ethical approval: Not applicable.

Data availability statement: No data associated in the manuscript.

References

(1) Singh VP, Badiger NM, Chanthima N, Kaewkhao J. Evaluation of gamma-ray exposure buildup factors and neutron shielding for bismuth borosilicate glasses. Radiat Phys Chem. 2014;98:14–21. doi: 10.1016/j.radphyschem.2013.12.029.

(2) Singh VP, Badiger NM, Kaewkhao J. Radiation shielding competence of silicate and borate heavy metal oxide glasses: Comparative study. J Non Cryst Solids. 2014;404:167–73. doi: 10.1016/j.jnoncrysol.2014.08.003.

(3) Oto B, Yıldız N, Akdemir F, Kavaz E. Investigation of gamma radiation shielding properties of various ores. Prog Nucl Energy. 2015;85:391–403. doi: 10.1016/j.pnucene.2015.07.016.

(4) Sayyed MI. Radiation shielding performance of amorphous silicates in the system SiO2-Na2O– RO (*R* = Cd, Pb or Zn). Silicon. 2023. doi: 10.1007/s12633-023-02671-5.

(5) Naseer KA, Marimuthu K, Mahmoud KA, Sayyed MI. Impact of Bi2O3 modifier concentration on barium–zincborate glasses: physical, structural, elastic, and radiation-shielding properties. Eur Phys J Plus. 2021;136:116. doi: 10.1140/epjp/s13360-020-01056-6.

(6) Issa SAM, Kumar A, Sayyed MI, Dong MG, Elmahroug Y. Mechanical and gamma-ray shielding properties of TeO2-ZnO-NiO glasses. Mater Chem Phys. 2018;212:12–20. doi: 10.1016/j.matchemphys.2018.01.058.

(7) Sayyed MI, El-Mesady IA, Abouhaswa AS, Askin A, Rammah YS. Comprehensive study on the structural, optical, physical and gamma photon shielding features of B2O3-Bi2O3-PbO-TiO2 glasses using WinXCOM and Geant4 code. J Mol Struct. 2019;1197:656–65. doi: 10.1016/j.molstruc.2019.07.100.

(8) ICRP. The 2007 Recommendations of the international commission on radiological protection. ICRP Publication 103. Ann. ICRP. Vol. 37; 2007. p. 2–4.

(9) Sayyed MI, Mahmoud KA, Islam S, Tashlykov OL, Lacomme E, Kaky KM. Application of the MCNP 5 code to simulate the shielding features of concrete samples with different aggregates. Radiat Phys Chem. 2020;174:108925. doi: 10.1016/j.radphyschem.2020.108925.
(10) Sayyed MI, Mahmoud KA, Tashlykov OL, Khandaker MU, Faruque MRI. Enhancement of the shielding capability of soda–-lime glasses with Sb2O3 dopant: A potential material for radiation safety in nuclear installations. Appl Sci. 2021;11:326. doi: 10.3390/app11010326.
(11) Hanfi MY, Sayyed MI, Lacomme E, Akkurt I, Mahmoud KA. The influence of MgO on the radiation protection and mechanical properties of tellurite glasses. Nucl Eng Technol. 2021;53(6):2000–10. doi: 10.1016/j.net.2020.12.012.
(12) Kilic G, Ilik E, Mahmoud KA, El-Agawany FI, Alomairy S, Rammah YS. The role of B_2O_3 on the structural, thermal, and radiation protection efficacy of vanadium phosphate glasses. Appl Phys A. 2021;127:265. doi: 10.1007/s00339-021-04409-9.
(13) Al-Saleh WM, Dahi MRH, Sayyed MI, Almutairi HM, Saleh IH, Elsafi M. Comprehensive study of the radiation shielding feature of polyester polymers impregnated with iron filings. e-Polymers. 2023;23(1):20230096. doi: 10.1515/epoly-2023-0096.
(14) Almuqrin AH, Yasmin S, Abualsayed MI, Elsafi M. An experimental investigation into the radiation-shielding performance of newly developed polyester containing recycled waste marble and bismuth oxide. Appl Rheol. 2023;33(1):20220153. doi: 10.1515/arh-2022-0153.
(15) Turner TA, Pickering SJ, Warrior NA. Development of recycled carbon fibre moulding compounds – Preparation of waste composites. Compos B Eng. 2011;42:517–25. doi: 10.1016/j.compositesb.2010.11.010.
(16) Adeosun SO, Lawal GI, Balogun SA, Akpan EI. Review of green polymer nanocomposites. J Miner Mater Charact Eng. 2012;11:385–416. doi: 10.4236/jmmce.2012.114028.
(17) Nagaraja N, Manjunatha H, Seenappa L, Sathish K, Sridhar K. Ramalingam H. Gamma, X-ray and neutron shielding properties of boron polymers. Indian J Pure Appl Phys (IJPAP). 2020;58:271–6.
(18) Lee S-Y, Kang I-A, Doh G-H, Yoon H-G, Park B-D, Wu Q. Thermal and mechanical properties of wood flour/talc-filled polylactic acid composites: Effect of filler content and coupling treatment. J Thermoplast Compos Mater. 2008;21:209–23. doi: 10.1177/0892705708089473.
(19) Qu P, Gao Y, Wu G-F, Zhang L-P. Nanocomposites of Poly(lactic acid) reinforced with cellulose nanofibrils. BioRes. 2010;5(3):1811–23.
(20) Kaushik A, Singh M, Verma G. Green nanocomposites based on thermoplastic starch and steam exploded cellulose nanofibrils from wheat straw. Carbohydr Polym. 2010;82:337–45. doi: 10.1016/j.carbpol.2010.04.063.
(21) Zadegan S, Hosainalipour M, Rezaie HR, Ghassai H, Shokrgozar MA. Synthesis and biocompatibility evaluation of cellulose/hydroxyapatite nanocomposite scaffold in 1-n-allyl-3-methylimidazolium chloride. Mater Sci Eng C. 2011;31:954–61. doi: 10.1016/j.msec.2011.02.021.
(22) Albarzan B, Almuqrin AH, Koubisy MS, Wahab EAA, Mahmoud KA, Shaaban K, et al. Effect of Fe_2O_3 doping on structural, FTIR and radiation shielding characteristics of aluminium-lead-borate glasses. Prog Nucl Energy. 2021;141:103931. doi: 10.1016/j.pnucene.2021.103931.
(23) Abouhaswa AS, Sayyed MI, Altowyan AS, Al-Hadeethi Y, Mahmoud KA. Synthesis, structural, optical and radiation shielding features of tungsten trioxides doped borate glasses using Monte Carlo simulation and phy-X program. J Non Cryst Solids. 2020;543:120134. doi: 10.1016/j.jnoncrysol.2020.120134.
(24) Dong MG, Tishkevich DI, Hanfi MY, Semenishchev VS, Sayyed MI, Zhou SY, et al. WCu composites fabrication and experimental study of the shielding efficiency against ionizing radiation. Radiat Phys Chem. 2022;200:110175. doi: 10.1016/j.radphyschem.2022.110175.
(25) Akman F, Ogul H, Ozkan I, Kaçal MR, Agar O, Polat H, et al. Study on gamma radiation attenuation and non-ionizing shielding effectiveness of niobium-reinforced novel polymer composite. Nucl Eng Technol. 2022;54:283–92. doi: 10.1016/j.net.2021.07.006.
(26) Hanfi MY, Sakr AK, Ismail AM, Atia BM, Alqahtani MS, Mahmoud KA. Physical characterization and radiation shielding features of B2O3As2O3 glass ceramic. Nucl Eng Technol. 2023;55:278–84. doi: 10.1016/j.net.2022.09.006.
(27) Howard CJ, Sabine TM, Dickson F. Structural and thermal parameters for rutile and anatase. Acta Crystallogr B. 1991;47:462–8. doi: 10.1107/S010876819100335X.
(28) Epp J. X-ray diffraction (XRD) techniques for materials characterization. Materials characterization using nondestructive evaluation (NDE) methods. Elsevier; 2016. p. 81–124. doi: 10.1016/B978-0-08-100040-3.00004-3.
(29) Mahmoud ME, El-Khatib AM, Badawi MS, Rashad AR, El-Sharkawy RM, Thabet AA. Fabrication, characterization and gamma rays shielding properties of nano and micro lead oxide-dispersed-high density polyethylene composites. Radiat Phys Chem. 2018;145:160–73. doi: 10.1016/j.radphyschem.2017.10.017.
(30) Sharma A, Sayyed MI, Agar O, Kaçal MR, Polat H, Akman F. Photon-shielding performance of bismuth oxychloride-filled polyester concretes. Mater Chem Phys. 2020;241:122330. doi: 10.1016/j.matchemphys.2019.122330.
(31) Mahmoud ME, El-Khatib AM, Badawi MS, Rashad AR, El-Sharkawy RM, Thabet AA. Recycled high-density polyethylene plastics added with lead oxide nanoparticles as sustainable radiation shielding materials. J Clean Prod. 2018;176:276–87. doi: 10.1016/j.jclepro.2017.12.100.
(32) Hou Y, Li M, Gu Y, Yang Z, Li R, Zhang Z. Gamma ray shielding property of tungsten powder modified continuous basalt fiber reinforced epoxy matrix composites. Polym Compos. 2018;39:E2106–15. doi: 10.1002/pc.24469.
(33) Farnaz Nasehi MII. Evaluation of X and gamma-rays attenuation parameters for polyacrylamide and ZnO composites as ligh. J Nucl Med Radiat Ther. 2019;10:1000404.
(34) Bagheri K, Razavi SM, Ahmadi SJ, Kosari M, Abolghasemi H. Thermal resistance, tensile properties, and gamma radiation shielding performance of unsaturated polyester/nanoclay/PbO composites. Radiat Phys Chem. 2018;146:5–10. doi: 10.1016/j.radphyschem.2017.12.024.
(35) Atta E, Zakaria KM, Madbouly A. Research article study on polymer clay layered nanocomposites as shielding materials for ionizing radiation. Int J Recent Sci Res. 2015;6:4263–9.
(36) Aldhuhaibat MJR, Amana MS, Jubier NJ, Salim AA. Improved gamma radiation shielding traits of epoxy composites: Evaluation of mass attenuation coefficient, effective atomic and electron number. Radiat Phys Chem. 2021;179:109183. doi: 10.1016/j.radphyschem.2020.109183.
(37) Akman F, Kaçal MR, Almousa N, Sayyed MI, Polat H. Gamma-ray attenuation parameters for polymer composites reinforced with BaTiO3 and CaWO4 compounds. Prog Nucl Energy. 2020;121:103257. doi: 10.1016/j.pnucene.2020.103257.
(38) Mahmoud KA, Tashlykov OL, Kropachev Y, Samburov A, Zakharova P, Abu El-Soad AM. A close look for the γ-ray attenuation capacity and equivalent dose rate form composites based epoxy resin: An experimental study. Radiat Phys Chem. 2023;212:111063. doi: 10.1016/j.radphyschem.2023.111063.